Excerpt from the Proceedings of the 2011 COMSOL Conference in Stuttgart

Xylophone Bar Magnetometry and Inertial-Grade MEMS Optimisation: A Multiphysics Approach

Harry T.D. Grigg*[1] and Barry J. Gallacher[1]
[1]Newcastle University

*Corresponding author: School of Mechanical and Systems Engineering, Stephenson Bldg., Claremont Road, Newcastle upon Tyne NE1 7RU, harry.grigg@newcastle.ac.uk

Abstract: This paper presents a snapshot of ongoing research aimed at development of a MEMS magnetometer capable of $nT/\sqrt{Hz}$ sensitivity over a wide dynamic range, along with its control system, in an integrated package. A design for a resonant magnetometer utilising a xylophone bar sense element(Fig.I) is proposed, analysed and optimised using classical techniques and COMSOL Multiphysics. As a starting point, the resonator is analysed using classical beam theory and Fourier analysis, with its control transducers modelled as parallel-plate capacitors, in a 2D context. Control behaviour is extracted by means of a multiple-timescale singular perturbation. The control behaviour and natural frequencies thus obtained are studied in COMSOL using a 3D Structural Mechanics based model.

The XBR Q factor and static compliance emerge from classical analysis as the critical design parameters influencing sensitivity. Thus motivated, a further COMSOL model is developed, coupling the 3D resonator analysis to a 2D PML model representing the substrate to which the XBR is attached. Using the above approach, the support Q is shown to be very high for XBR-type resonators as compared to more traditional beam designs. With appropriate choice of geometry, achieving thermoelastically limited overall Q is seen to be possible. The effect of applying a sense current is studied via the Joule Heating physics interface, and the temperature-dependence of the mode shapes, frequencies, and Q factors is examined in this context. These results are benchmarked against standards from the literature, exhibiting close agreement.

Taken together, the results of the COMSOL modelling and dynamical analysis of the device under parametric drive imply that the concept of a parametric XBR holds out the promise of realising an inertial grade MEMS magnetometer with $nT/\sqrt{Hz}$ sensitivity. The commercial impact of such a sensor would be profound and immediate, opening up whole new application classes. Further work is necessary to determine whether the theoretical potential $pT/\sqrt{Hz}$ sensitivity can be achieved, which would open up countless applications in the growth market of biomedical field detection .

Keywords: Support Loss, MEMS, XBR, High Q, parametric amplification.

---

1. Introduction

3D vector magnetometers are ubiquitous in fields and devices as diverse as aerospace, military applications, robotics, and geomagnetics, as well as in the rapidly expanding handheld navigation and modern smartphone markets. Typically, they are employed in an IMU to negate zero-point accelerometer drift.

There exists a performance dichotomy between high-performance macroscopic inertial grade magnetometers and automotive grade MEMS more often found in vehicles, smartphones, and consumer electronics. The former possess the necessary field sensitivity for precision navigation while the latter do not. For a precision IMU, a typical sensitivity specification is on the order of 1-10 $nT/\sqrt{Hz}$. Current MEMS magnetometers are orders of magnitude away from achieving inertial grade performance[1]; demand exists for inertial MEMS magnetometers inasmuch as their realisation would vastly expand the scope of precision inertial navigation, with applications to guided projectiles, indoors/ underground navigation, aerospace/spaceflight, and other areas.

.

1.1 Resonant sensors and the Xylophone bar Magnetometer

Resonant sensing refers to the technique of using a high-Q resonator as the sense element and arranging operation such that the phenomenon of interest drives the resonator at its natural frequency. The advantage lies in the

fact that the resonator selectively stores energy at its natural frequency, increasing the sensitivity to the effect of interest by the Q factor, which can exceed 10^6, while rejecting off-resonance noise spectral components.

The Xylophone Bar Magnetometer was developed at Johns Hopkins University in the 1990s[2]. The fundamental concept is to attach the supports in such a way as to make the impedance seen by the wave modes of interest as large as possible, ideally infinite. This condition, in the limit, results in total reflection of the wave at the support-resonator interface, and hence zero energy leakage to the environment via this mechanism[3].

The XBR realises this condition by attaching the supports at the predicted node points of the first mode of the resonator considered under free boundary conditions.

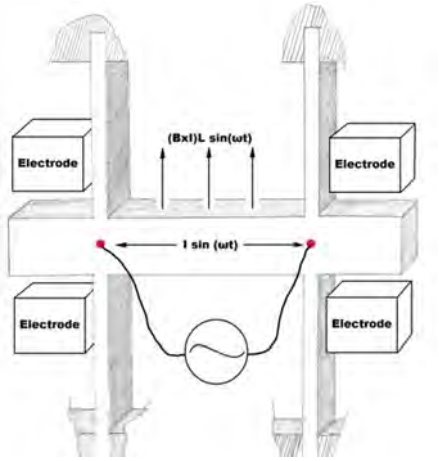

Fig. I: Schematic representation of resonator geometry and operating principle of an XBR. The electrodes carry a time dependent voltage V(t).

2. Resonator System Dynamics

2.1. Beam dynamics

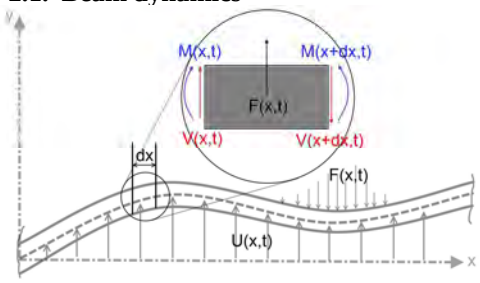

Fig.II: Terminology and sign conventions for analytical purposes**.**

With reference to Fig.II, the potential and cokinetic energies of a free-free beam under electrostatic actuation can be readily found as:

$$T^* = \frac{\rho A}{2}\int_0^L \dot{U}^2 dx$$

$$V = \frac{1}{2}\int_0^L M^2 dx + \frac{\varepsilon_0 w}{2} V_{BIAS}\int_0^L U^2 dx$$

Assuming linear damping via a Rayleigh dissipation function and applying the extended Euler-Lagrange equation, we arrive at the system equations of motion:

$$EI\,\frac{\partial^4 U}{\partial x^4} + \rho A_x \frac{\partial^2 U}{\partial t^2} + C\frac{\partial U}{\partial t} = F(t)$$

Applying separation of variables and Fourier's method with free boundary conditions, the mode shapes are obtained as

$$X_n(x) = C_n\Big[sin\beta_n x + sinh\beta_n x + \Big[\frac{sinh\beta_n L - sin\beta_n L}{cos\beta_n L - cosh\beta_n L}\Big](cosh\beta_n x - cos\beta_n x)\Big]$$

And the generalized coordinate corresponding to mode I can be shown to obey

$$\ddot{q} + \varepsilon\upsilon\omega_1\dot{q} + \omega_1^2\{1 - \varepsilon(V_1^2 + V_2^2)\}q + \varepsilon K_1(V_1^2 + V_2^2)q^2 - \varepsilon K_2(V_1^2 + V_2^2)q^3 = \varepsilon fI + \varepsilon g(V_1^2 - V_2^2)$$

2.2. Parametric amplification

Parametric amplification refers to the exploitation of parametric resonance in a resonator to increase the sensitivity of the system to external harmonic stimuli at the natural frequency of interest. For a detailed exposition of the topic in the context of resonant sensors, see[4].

In order to excite primary parametric resonance and to force the device at its fundamental mode, we choose the frequency components of V(t) to include $\frac{\omega_1}{2}$and $2\omega_1$, where ω_1 is the natural frequency of Mode I of the beam under free boundary conditions.

Taking the parametric strength ε to be small relative to the mechanical stiffness of the first mode, this quantity can be used as a basis for a multiple timescales asymptotic approximate solution to (II). Application of this perturbative technique yields the approximate equation of motion for the first generalized coordinate as

$$A_0 = \frac{i|F|}{2} QG$$

Where $G$is a nonlinear function encoding the parametric strength, becoming unbounded as the strength approaches a critical value, F is the forcing term, and Q is the system quality factor.

To give the above result some physical meaning, observe that the response amplitude is proportional to the static compliance of the device, to the resonator Q factor, and to G. G acts to multiply Q in a smooth, scalar fashion, which is equivalent to reducing the effective damping in the system.

3. Design for Q

3.1. Sources of dissipation

The Q factor is defined such that it is proportional to the reciprocal of the dissipation. Hence, independent dissipative contributions sum in a linear fashion, and the Q factors from N dissipation sources combine according to

$$\frac{1}{Q_{TOTAL}} = \sum_{i=1}^{N} \frac{1}{Q_i}$$

Some important contributions for the present case are considered below to put the subsequent modeling in its proper context.

3.1.1. Gas damping

For beam resonators operating under atmospheric conditions, gas damping effects are generally dominant. In particular, cyclic viscous pumping of the thin layer trapped between the resonator and a capacitive actuator or sensor is significant. It can be shown[5] that, to a good approximation, in a rarefied atmosphere typical of modern vacuum packaged devices,

$$Q_{gas}^{-1} = (2\pi)^{2/3} \frac{2(L+b)P}{h\omega_1 \rho h_0} \sqrt{\frac{M_{mol}}{RT}}$$

For high-performance devices where packaging costs do not dominate, modern wafer-level hermetic technology allows for operation under high vacuum in the field, largely negating this effect.

3.1.2. Thermoelastic damping(TED)

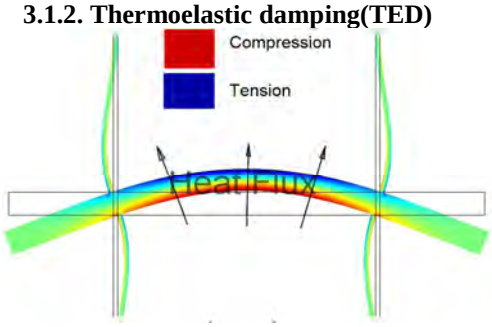

Fig. 3: Mechanism of TED in an XBR, illustrated via a 2D COMSOL eigenfrequency analysis.

Thermoelastic damping of a resonator describes the loss of usable energy to irreversible heat transfer that is driven by elastic strain-induced temperature gradients in the material[6]. The following approximation agrees very well with experiment:

$$Q_{TED}^{-1} = \frac{(1-2\nu)(C_p - C_v)(\omega\mu)}{3C_v(\omega^2 + \mu^2)}$$

This constitutes a hard limit on the Q factor; the theoretical potential sensitivity of a given resonator geometry is approached asymptotically as other dissipation contributions are made smaller than this value.

3.1.3. Support loss

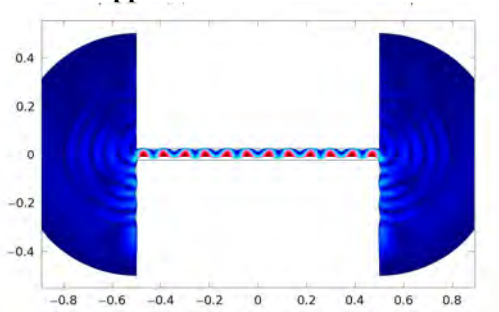

Fig. 4: Mechanism of support loss, illustrated through a simple 2D time-dependant COMSOL simulation of a clamped-clamped beam resonator connected to linear isotropic elastic substrates, modelled as infinite by the addition of a PML. A higher order transverse mode is shown,

Momentum transport by means of wave radiation into the resonator substrate constitutes a source of dissipation termed support loss. After controlling ambient pressure to mitigate gas effects, support loss can often be the dominant source of dissipation for beam resonators[3]. However, it is highly

sensitive to resonator geometry; indeed, the purpose and advantage of an XBR over other geometries lies in the reduced support losses on offer, as suggested above. Hence, a quantitative understanding of support loss in XBRs is critical to optimizing the performance of an XBM.

3.2. Substrate wave modelling

The mechanical radiation that constitutes support loss consists of displacement waves propagating in the substrate to which the resonant element is anchored. For MEMS devices, this is typically a planar structure many orders of magnitude larger than the resonator; hence, boundary effects and reflections can be neglected, and it is safe to assume that all energy leaving the resonator via mechanical coupling to the substrate is lost to the environment. On this basis, an appropriate model for the substrate is an infinite elastic half-plane.

3.2.1: Analytical models

The physics of isotropic linear elastic wave propagation in such a domain has been examined in the past, with Miller and Pursey[7] deriving closed-form exact analytical expressions for the total energy flux from a narrow distributed radiation source on the free surface of the half plane.

These expressions have been used[8] to estimate the support Q for C-C and cantilever beams, with good experimental agreement. This was done by considering only shear forces at the substrate-resonator interface, the moments and normal forces being negligible for that particular case. However, the very purpose of the XBR is to reduce towards zero the forces experienced at the interfaces of its support beams with the substrate; any model capturing the effect of XBR geometry must therefore include shear and normal forces, the effects of which can be superposed owing to the linearity of the problem.

It only remains, then, to obtain expressions for the normal and shear interface forces at the support interfaces of the XBR to complete an analytical model of XBR support loss.

3.2.2: COMSOL anisotropic PML model

The analytical approach outlined above describes the planar isotropic case to a good approximation. However, for a MEMS implementation, the anisotropy of Si will lead to deviations from this model in implementation. An analytical model dealing with the anisotropic elasticity would be unwieldy, but COMSOL and the FEM can handle this behavior naturally.

3.3. Dissipation modeling approach: validation

Hao et al. derived the following expressions for the Q factor associated with the nth mode of a clamped-free and clamped-clamped beam, respectively:

$$Q_{C-F(n)} = \left[\frac{0.24(1-\upsilon)}{(1+\upsilon)\Psi}\right]\frac{1}{(\beta_n\chi_n)^2}\left[\frac{L}{b}\right]^3$$

$$Q_{C-C(n)} = \left\{\frac{2.43}{(3-\upsilon)(1+\upsilon)} + \frac{1.91}{\Pi}\right\}\frac{1}{(\beta_n\chi_n)^2}\left[\frac{L}{b}\right]^3$$

Cantilevers of fixed length and parametrised height in the plane of vibration were chosen as test cases and implemented parametrically in COMSOL as validation for the modeling procedure.

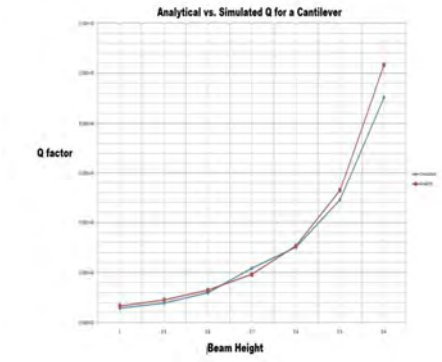

Fig. 5: Comparison of COMSOL PML simulation of a cantilever resonator with analytical result from Hao et al. Note agreement within 10 percent over an order of magnitude. Good agreement is seen; this supports the validity of the COMSOL modelling.

3.4.Dissipation modeling I: XBR modal dynamics

The model developed in Section 2 delivers useful insight into the control behavior of the resonator, and supplied the motivation to investigate the Q factor as important design parameter. However, since it assumes perfectly compliant supports, it has nothing to say about support loss, which occurs precisely due to imperfect substrate-resonator decoupling. A model including the dynamics of the support beams is required for this purpose, and is developed in the sequel.

3.4.1. XBR Rayleigh-Ritz model

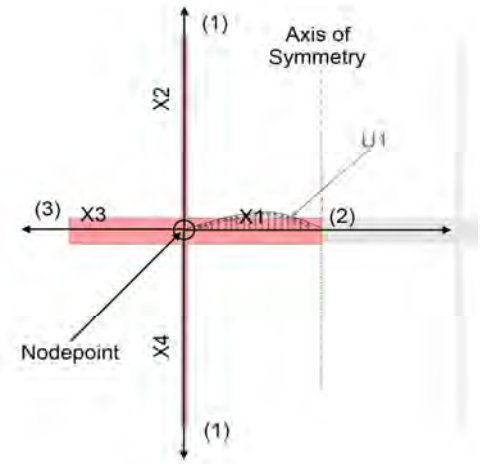

Fig. 6: Geometry, boundaries,, fields and coordinates for XBR Rayleigh-Ritz approximation.

The XBR can be analysed by defining spatial variables $X_i, i \in \{1,2,3,4\}$ and corresponding Euler-Bernoulli fields U_i, as indicated in Fig. 6. Exploiting the symmetric geometry of the resonator and applying appropriate boundary conditions, as given in Table 1 below, and assuming complex-exponential trial functions, the Rayleigh-Ritz method gives a tractable, analytical approximation for the system.

This quasi-1D model gives the required approximations for the shear and normal forces at the distal ends of the support beams ((1) in Fig. 6). See Sect. 3.5.2 for a comparison of the solutions yielded by the two approaches.

3.4.2. COMSOL Thermoelectromechanical (TEM) model

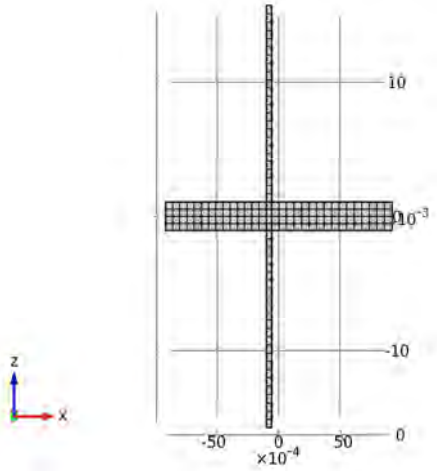

Fig. 7. COMSOL swept mesh of XBR geometry**. This simple configuration was found to promote rapid convergence, due to excellent minimum element quality properties.**

To attack the same problem in COMSOL, a fully parametric model of one half of the resonator geometry was developed, using the same symmetry exploited in Sect.3.4.1, as shown in Fig.7.

Boundary	**Solid Mechanics B.C. in COMSOL**	**Analytical B.C.(Fig. 6)**
Support Interface(1)	Fixed	$U_i = 0, U_i' = 0$ $i \in \{1,2,3,4\}$
Symmetry boundary(2)	Symmetry	$U_2\|_L = 0,$ $U_2'\|_L = 0$
Node point	Internal (FE continuity)	Slope Continuity, no displacement
All other boundaries(3)	Free	$U_i'' = 0, U_i''' = 0$ $i \in \{1,2,3,4\}$

Table 1: Comparison of analytical and COMSOL boundary conditions for mechanical models.

This approach incorporates more effects of interest than the Rayleigh-Ritz approach given in Sect. 3.4.1. In particular, the multiphysics capability of COMSOL facilitates modeling of the temperature dependence of the material properties of the resonator and the resulting interaction between applied sense current and the XBR dynamics.

3.5. Multiphysics coupling: Joule Heating

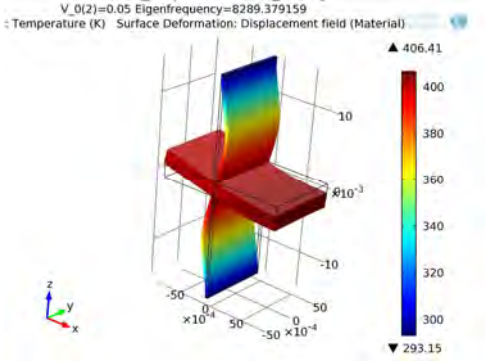

Fig. 8: COMSOL plot of coupled thermoelectromechanical model. Colour denotes temperature: deformation corresponds to the deflection field U.

The XBM, in contrast to most other micromagnetometers, can achieve a dynamic range spanning 9 or more orders of magnitude, from 1 T or larger electromagnet fields down to the nT level discussed. This is achieved by controlling the product of the field strength and the sense current to remain within an order of magnitude of a nominal value, and in the small field limit is constrained only by the

applicable sense current. Hence it is of interest to examine the relationship between the applied sense current, the temperature distribution in the device, and the dynamic response.

This was realized by using a 2-stage segregated solver: first, the Joule Heating interface and a Stationary study was employed to model current flow and resultant heat generation in the device, as a function of the driving voltage parameter; secondly, a variable corresponding to an approximation for the thermal dependence of the Young's modulus was defined and used to define the material properties in the Structural Mechanics model described in Sect.3.4, and the model solved using an eigenfrequency analysis.

Fig. 9: COMSOL plot of XBR mode shapes for different values of the sense current. Joule heating effects result in inhomogeneous stiffness, leading to the observed change in mode shapes.

3.5.1 Effect on operating Q

To obtain respective estimates of the support Q from the analytical and COMSOL models, it is necessary to translate the calculated interface forces to a corresponding rate of dissipation. This is achieved via the use of the approach outlined in Sect.3.2.1 and Sect.3.4.1 for the analytical model, and using the PML method of Sect. 3.2.2 for comparison.

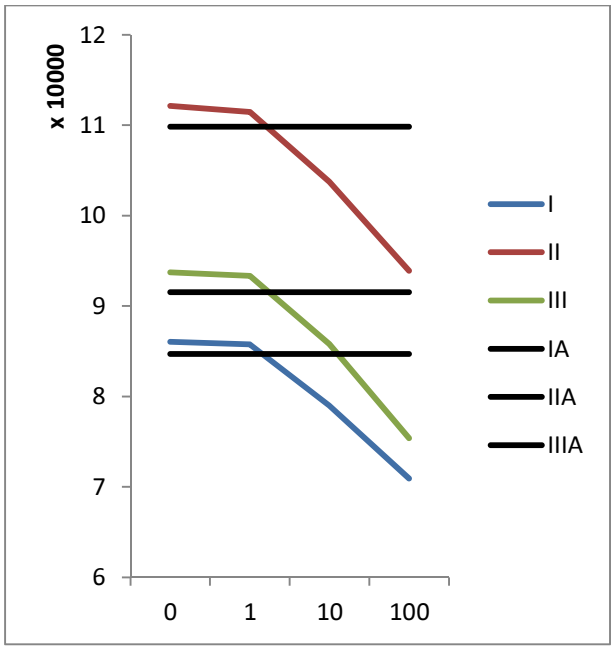

Fig. 10: Plot superposing analytical prediction of device Q factors with COMSOL estimate. The independent variable is applied sense voltage; the dependent variable is support Q factor. The black plots indicate analytical predictions; the coloured plots indicate the corresponding COMSOL results. Series I, II, and III correspond to different geometries (small perturbations of the support width around the tuned value).

Good agreement is observed between the two models over a range of geometries when no sense current is applied in the COMSOL model (and hence Joule Heating effects are neglected), as can be seen in Fig. 10. A substantial drop in support Q is seen as the applied sense current rises.

3.4.3 Design implications

The nominal dimensions of the model and first prototype were tuned for maximum Q using the analytical model given in Sect. 3.4.1. Permutations of small geometric changes in the above model were iterated using a Parametric study, fine-tuning the model to account for the effects of Joule Heating and variable material properties. It was found that at higher applied voltages, the optimal attachment point moved towards the distal ends of the sense beam. Additionally, the results required retuning of the natural frequencies such that the support beam natural frequency of interest was slightly lower than that of the sense beam, due to the larger temperature increase and hence softening effect in the latter. This is in contrast to the

analytical model, which suggests perfect mode-tuning as the optimal condition.

4. Conclusion

The steady-state system response is given in Sect.2.2, as a function of forcing strength, parametric pumping, and classical Q factor. The forcing per unit applied field is well known as the cross-product of the sense current and the ambient transverse flux density, integrated over the sense element. The field sensitivity of the device as a magnetometer corresponds to the minimum change in response detectable, which is a known function of the control electronics. Using the tuned Q factors from Fig.10 and the parametrically amplified response amplitude expression , and assuming a parametric gain G of 100, the response amplitude enters the 1-second detectable range at a field strength of $734\,pT$. Hence, the field resolution with a sampling interval of 100 Hz is estimated to be $7.34\,nT$ – sufficient for true inertial-grade performance.

5. References

1. **Lenz, J. and S. Edelstein, *Magnetic sensors and their applications.* Sensors Journal, IEEE, 2006. 6(3): p. 631-649.**
2. **Givens, R.B., et al., *A high sensitivity, wide dynamic range magnetometer designed on a xylophone resonator.* Applied Physics Letters, 1996. 69(18): p. 2755-2757.**
3. **Grigg, H.T.D., Gallacher, B.J., *Towards a Parametrically Pumped Xylophone Microbar Magnetometer: Design Optimisation of Xylophone Bar Resonators*, in *IMAPS Device Packaging Conference 2011*. 2011, IMAPS Press: Phoenix, AZ.**
4. **Gallacher, B.J., J.S. Burdess, and K.M. Harish, *A control scheme for a MEMS electrostatic resonant gyroscope excited using combined parametric excitation and harmonic forcing.* Journal of Micromechanics and Microengineering, 2006. 16(2): p. 320-331.**
5. **Bao, M. and H. Yang, *Squeeze film air damping in MEMS.* Sensors and Actuators A: Physical, 2007. 136(1): p. 3-27.**
6. **Zener, C., *Internal Friction in Solids. I. Theory of Internal Friction in Reeds.* Physical Review, 1937. 52(3): p. 230.**
7. **Miller, G.F. and H. Pursey, *The Field and Radiation Impedance of Mechanical Radiators on the Free Surface of a Semi-Infinite Isotropic Solid.* Proceedings of the Royal Society of London. Series A, Mathematical and Physical Sciences, 1954. 223(1155): p. 521-541.**
8. **Hao, Z., A. Erbil, and F. Ayazi, *An analytical model for support loss in micromachined beam resonators with in-plane flexural vibrations.* Sensors and Actuators A: Physical, 2003. 109(1-2): p. 156-164.**

6. Acknowledgements

This work was funded by an EPSRC grant. Additionally, the authors would like to express their gratitude to Ritchie Burnett, Jim Burdess, Xhongzhu Hu, and the rest of the Newcastle Microsystems group, without whom this research would not have been possible.